Study of a flexible UAV proprotor

Fazila Mohd Zawawi, Peng Lv, Sebastien Prothin, Joseph Morlier, Jean-Marc Moschetta, Emmanuel Bénard

Study of a flexible UAV proprotor

Fazila Mohd-Zawawi*, Peng Lv and Sebastien Prothin

Département Aérodynamique, Energétique et Propulsion (DAEP),
Institut Supérieur de l'Aéronautique et de l'Espace,
Toulouse 31000, France
E-mail: fazila.mohd-zawawi@isae.fr
E-mail: peng.lv@isae.fr
E-mail: sebastien.prothin@isae.fr
*Corresponding author

Joseph Morlier

ICA, ISAE/INSA/UPS/ENSTIMAC,
Université de Toulouse,
10 av. Edouard Belin,
BP 54032 – 31055 Toulouse Cedex 4, France
E-mail: joseph.morlier@isae.fr

Jean-Marc Moschetta and Emmanuel Benard

Département Aérodynamique, Energétique et Propulsion (DAEP),
Institut Supérieur de l'Aéronautique et de l'Espace,
Toulouse 31000, France
E-mail: jean-marc.moschetta@isae.fr
E-mail: emmanueal.benard@isae.fr

Abstract: This paper is concerned with the evaluation of design techniques, both for the propulsive performance and for the structural behaviour of a composite flexible proprotor. A numerical model was developed using a combination of aerodynamic model based on blade element momentum theory (BEMT), and structural model based on anisotropic beam finite element, in order to evaluate the coupled structural and the aerodynamic characteristics of the deformable proprotor blade. The numerical model was then validated by means of static performance measurements and shape reconstruction from laser distance sensor outputs. From the validation results of both aerodynamic and structural model, it can be concluded that the numerical approach developed by the authors is valid as a reliable tool for designing and analysing the UAV-sized proprotor made of composite material. The proposed experiment technique is also capable of providing a predictive and reliable data in blade geometry and performance for rotor modes.

Keywords: convertible aircraft; fluid-structure-interaction; micro air vehicles; flexible proprotors; low Reynolds number; blade element momentum method; rotating coupled timoshenko beam; anisotropic finite element; laser distance sensor; LDS.

Reference to this paper should be made as follows: Mohd-Zawawi, F., Lv, P., Prothin, S., Morlier, J., Moschetta, J-M. and Benard, E. (2014) 'Study of a flexible UAV proprotor', *Int. J. Engineering Systems Modelling and Simulation*, Vol. 6, Nos. 3/4, pp.149–161.

Biographical notes: Fazila Mohd-Zawawi received her Bachelor degree in Mechanical Engineering from the Universiti Teknologi Malaysia (UTM) in 2003 and Master degree in Aeronautical Engineering from the Institut Supérieur de l'Aéronautique et de l'Espace (ISAE, Toulouse, France) in 2010. She is currently doing her PhD at the same university as where she did her master studies, researching on aeroelastic of flexible blades for tilt-body micro air vehicles (MAV) proprotors. Before starting ISAE graduate school, she worked one year at UTM under the Department of Aeronautics as an Assistant Lecturer. Within that one year, she was involved in research on aerodynamic of heavyweight vehicles under the effect of crosswind, also on Malaysian National Car, called Proton, besides giving lectures and tutorial classes to bachelor students. She is going to continue serving as a Lecturer at UTM once she finished her PhD. Her research interests include MAV design, aerodynamic applications, proprotor aeroelastic analysis and design optimisation, computational fluid dynamics (CFD), computational structural dynamics (CSD) and MAV's propulsion systems.

Peng Lv is currently studying for PhD in his third year at Institut Supérieur de l'Aéronautique et de l'Espace of France (ISAE), researching on the flexible proprotor blades of MAV, focusing on the experimental aspect. He obtained his Master degree from Northwestern Polytechnical University, China in 2011. His research interests include flow field, stationary deformation and dynamics of rotating flexible blades.

Sebastien Prothin's research focuses on the application of multidisciplinary approaches to the development of rotor cutting-edge technologies at MAV scale, with emphasis on aerodynamics. His current research projects within the APMD group at ISAE include electro-actuated rotor blades, passively-adaptive rotor blades, bio-inspired nano-rotors, flapping-rotors and confined rotors. He developed skills in experimental fluid mechanics (wind tunnel, loads and PIV measurements) and structural analysis (deformation and displacement measurements).

Joseph Morlier is currently a Professor in Structural Mechanics at ISAE. He started working for ISAE-SUPAERO in November 2006 as an Associate Professor in Structural Mechanics and Structural Dynamics. From September 2005 to June 2006 he was Lecturer in Scientific Computing and Matrix Computations at University of Bordeaux 1. He was invited as a Researcher at LIAMA (Sino French Laboratory in Computer Science, Automation and Applied Mathematics), Beijing China in Summer 2006. He successfully defended his PhD titled 'Mode shape analysis using signal processing for in situ structural diagnosis' in December 2005. In November 2001, he received his Master's degree in Mecatronics and Signal Processing from University of Bordeaux 1. His current researches at ISAE and Institut Clément Ader focus on structural health monitoring (damage identification in composites, pattern recognition), structural and multidisciplinary optimisation (surrogate modelling, model updating, fluid structure interaction) and modal identification (vibration signal processing, mode shape identification).

Jean-Marc Moschetta is a Professor of Aerodynamics in the Department Aerodynamics, Energetics and Propulsion at the Institut Supérieur de l'Aéronautique et de l'Espace (ISAE). He graduated from SUPAERO in 1987. He received his PhD in 1991 and received the Habilitation thesis in 2000. In 1994–1995, he was invited as a Visiting Professor at Caltech, California. In 2011, he founded the Micro Air Vehicle Research Centre in Toulouse which now networks nine research laboratories involved in MAV technologies.

Emmanuel Benard works in the Aerodynamics and Propulsion Department of the Institut Supérieur de l'Aéronautique et de l'Espace of France (ISAE), one of the most prominent aerospace schools in Europe. He is the Leader of the Advanced Aerodynamics and Flow Control research group and has years of experience in experimental fluid dynamics and unsteady aerodynamics.

1 Introduction

Tilt-rotor aircraft has been developed to be multifunctional in order to offer a wide range of services. It can fly in both of hover and forward flight. In early 1950s, tilt-rotor aircraft has started to be developing. XV-3 of Bell company operated first transition from hover to forward flight. In 1970s, XV-15 was developed by Bell company to demonstrate the feasibility of tilt-rotor concept. Then it was moved to NASA and the US Army for further study in aeroelasticity. The success of XV-15 led to the project of V-22. V-22 is the world's first production tilt-rotor aircraft. Likewise, the tilt-body concept of typical aircraft attracts interest of researchers who are working on MAVs. In 2008, the efforts on the aerodynamic design of a tilt-body MAV named mini-Vertigo was introduced (Shkarayev et al., 2008). The results obtained in the study were realised in the design of a prototype of tilt-body MAV which was successfully tested in flight. With respect to a proprotor for tilt concept aircraft, in hover, the inflow velocity is small and the proprotor must provide high thrust to support aircraft weight. By contrast, in forward flight, the inflow velocity is relatively large and the low thrust is just to overcome the drag. The difference in the inflow and thrust requirement between the two flight modes suggests different blade twist and chord distributions. McVeigh and Rosenstein (1983) obtained the twist of XV-15 proprotor through linear interpolation of twist between rotor and propeller by a compromise. Although this trade-off provided acceptable performance on XV-15, the stiff proprotor with certain twist cannot maximise the efficiency for both flights. In 1988, a passive blade twist control method for the proprotor of XV-15 was proposed (Nixon, 1998). The study demonstrated successfully the feasibility of the passive blade control on conventional tilt-rotor aircraft. The small proprotors also

suffer the problem caused by different twist between hover and forward flight. However, due to the small size of MAV, the complex tailored blade cross section for passive twist control based on conventional tiltrotor aircraft is not available anymore on it. Therefore, composite laminate is explored to be a more practical method for proprotor blade of MAVion, which is a tilt-body MAV developed by ISAE, due to their potential benefits such as aeroelastic tailoring, ability to manufacture, more refined aerodynamic designs, significant enhancements in fatigue performance and damage tolerance of the blade. The blade is expected to be deformed in torsion under different airloads and structural loads. In this study, a passive twist control is considered as a potential way to improve the overall flight efficiency of MAV proprotor as it is expected by numerical design to offers $\sim 30\%$ increment of total efficiency in hover as compared to the proprotor designed in targeted cruise point (Mohd-Zawawi et al., 2012). Hence, this paper is aimed at developing an evaluation of design techniques of a composite flexible proprotor.

2 Numerical model

2.1 Aerodynamic model (FPROP)

The aerodynamic model based on BEMT is used as a tool to compute the aerodynamic loadings in terms of lift force, drag force and pitching moment around quarter of the chord distributed in spanwise. The quasi-steady aerodynamic loading is calculated using a two-dimensional aerodynamic theory in a strip-manner. In the aerodynamic modelling for both forward flight and hover case, the classical BEMT is used. In this model, the flow angle is iteratively computed until the convergence criteria are reached. This iterative analysis procedure determines the characteristics of a given proprotor (C_T, C_P) and its corresponding performance [$\eta_{proprotor}$ (forward flight case) or FM (hover case)]. The axial induced velocity (vi_a),tangential induced velocity (vi_t), and Reynolds number (Re) depending on the operating condition are also iteratively computed in the analysis process. The BEMT procedure of FPROP is shown as a block diagram in Figure 1 and the detailed equations for both flight modes are described in Subsection 2.2.

In the classical approach of low order proprotor analysis, different assumptions are used, i.e., lift polar is a linear function, in order to obtain a closed loop solution or even to quickly converge the iterative process. Hence, in order to consider non-linear airfoil characteristics prevalent in low Reynolds number regime (Re $< 70,000$), XFOIL, an airfoil analysis code designed for low Reynolds number, developed by Drela (1989) was integrated into the design iterative process to eliminate this assumption as well as to precisely compute the aerodynamic coefficients.

Figure 1 BEMT procedure in FPROP

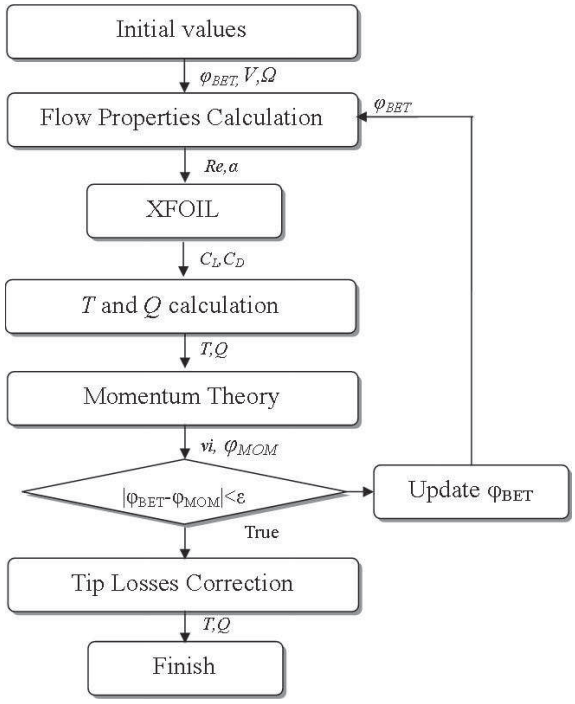

It is known that the airfoil performance is dependent to Reynolds number. The aerodynamics of airfoils varies rapidly with their configuration when the Reynolds number is on the order of 10^5. From the experiments done by Jones (1990), showed that a thin flat plate is inferior to a conventional shaped airfoil when Re = 1.2×10^5, but superior when Re = 4×10^4. Sunada et al. (1997) concluded that a flat plate with a thickness ratio of 5% has larger lift slope than conventional streamlined airfoils. Hence, due to the mentioned fact, flat plate profile was chosen to be used in the blade for MAV. Other than that, the use of flat plate in this study is due to the fact that the composite laminate was employed to enable the blade deformation for the purpose of proprotor performance enhancement. Flat plate also can reduce its sensitivity to the turbulence level variation (Hein and Chopra, 2007) as can be illustrated in Figures 2 and 3. In this respect, the n_{crit} parameter, used to define the turbulence level in XFOIL, can be set as 0.1 for both flight modes. However, to obtain a more precise evaluation of proprotor characteristics in forward flight, n_{crit} was set as 9. The developed iterative process of analysis procedures using BEMT method was validated with the QPROP (Drela, 1990) and the experimental measurement.

2.2 Blade element momentum theory

The momentum theory is an integral approach where the control volume is split into elements as shown in Figure 4.

Figure 2 Aerodynamic coefficients of flat plate at Re = 50,000 (see online version for colours)

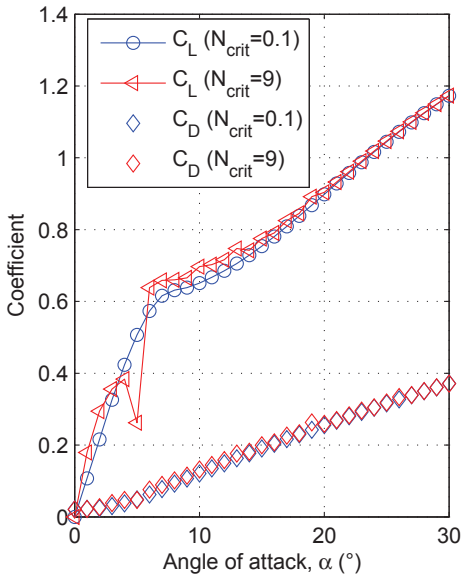

Figure 3 Aerodynamic coefficients of NACA0012 at Re = 50,000 (see online version for colours)

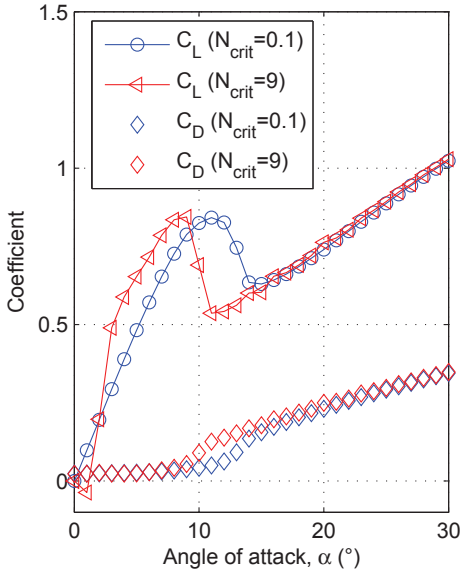

Figure 4 Control volume in momentum theory

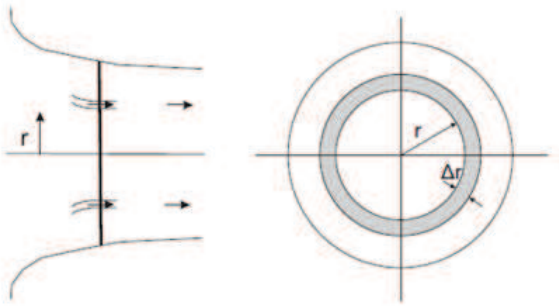

According to the momentum theory of propeller, the axial component of velocity in the plane of propeller is $V(1+a)$, where a is the axial inteference factor, and the axial component of velocity far behind propeller is $V(1+2a)$. Mass flow through the annulus of the disc is defined by equation (1).

$$m' = \frac{dm}{dr} = 2\pi r \rho V(1+a) \tag{1}$$

Figure 5 Simple actuator disc theory

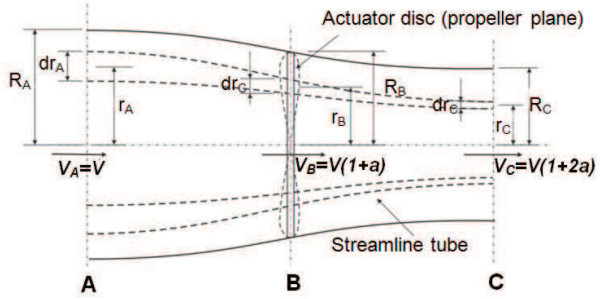

Thrust dT of the annulus can be expressed as $2VaFdm$, where F is momentum loss factor (correction for the momentum losses due the propeller blade tip effect). In order to avoid unconverged solution for rotor case ($V = 0$) due to the linked term of interference factor with the inlet velocity, axial induced velocity (vi_a) is solved in FPROP instead of interference factor. Therefore, thrust acting on the annulus can be expressed by equation (2).

$$T' = \frac{dT}{dr} = 2\pi r \rho (V + vi_a)(2vi_a F) \tag{2}$$

According to the momentum theory of propeller, radial component of velocity in the plane of the propeller is $\Omega r(1-a')$, where a' is the radial inteference factor, and radial component of velocity far behind the propeller is $\Omega r(1-2a')$. Torque needed for rotation of the annulus can be expressed by (3).

$$\frac{Q'}{r} = d\frac{\frac{Q}{r}}{dr} = 2\pi r \rho (V + vi_a)(2vi_t F) \tag{3}$$

where vi_t is the tangential induced velocity.

An expression for the elemental thrust and torque generated by a blade element can be written as in equations (4) and (5), respectively.

$$T' = L' \cos\phi - D' \sin\phi = L' \cos\phi(1 - \varepsilon \tan\phi) \tag{4}$$

$$\frac{Q'}{r} = L' \sin\phi + D' \cos\phi = L' \sin\phi(1 + \varepsilon \tan\phi) \tag{5}$$

where L' is the lift elemental lift, D' is the elemental drag and ε is the elemental drag-to-lift ratio, whose the respective expressions are as follow:

$$L' = \frac{1}{2}\rho c_L c W^2 dr \tag{6}$$

$$D' = \frac{1}{2}\rho c_D c W^2 dr \tag{7}$$

where W is the resultant velocity.

$$\varepsilon = D'/L' \tag{8}$$

Figure 6 Blade element theory

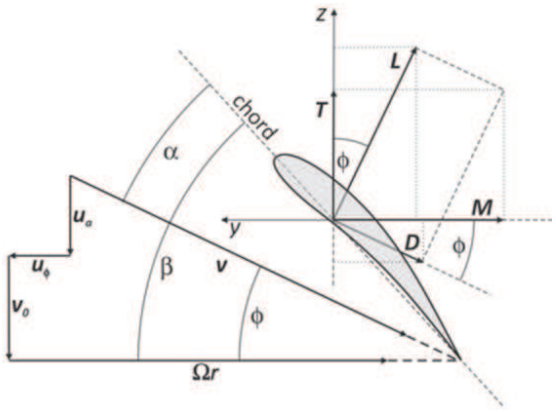

Combining the blade element theory and momentum theory results in the BEMT and allows to determine the real angle of attack and inflow velocity and thus the real thrust and torque of the rotor.

Since the BEMT does not incorporate the reduced lift distribution close to the tips, thus a tip loss model has to be used to cover this effect. In FPROP code the Prandtl's approach is used. The Prandtl relation that represents the momentum loss factor is described as:

$$F = \frac{2}{\pi}\arccos(e^f) \tag{9}$$

$$f = \frac{B}{2}\left(1 - \frac{r}{R}\right)\frac{1}{\lambda_w} \tag{10}$$

$$\lambda_w = \frac{r}{R}tan\phi \tag{11}$$

2.3 *Validation of FPROP*

For validation purposes, a 2-bladed rotor with rectangular planform (R = 0.1 m, c = 0.02 m), flat plate blade profile with thickness t/c = 2.5% and blade pitch of 25° was used in the aerodynamic model validation for a case without inflow (hover case). Meanwhile, the propeller APC 8 × 6 was used to validate the FPROP for forward flight case. The inflow velocity was 16 m/s. The result validation of BEMT for hover and forward flight cases in terms of thrust and torque are shown in Figures 7 and 8, respectively. From the validation result, it is found that the developed BEMT method with the integration of XFOIL shows better agreement with the experimental measurement compared to QPROP. QPROP, a propeller analysis tool with simplification of linear lift polar, showed unacceptable results due to its incapability to predict aerodynamic coefficients at post-stall angle of attacks. Likewise, an uncertainty in evaluating precise results might occur due to this limitation especially in post-stall blade. A slight increase in torque observed in the experimental result is possibly due to the heavy material (aluminium) used in the blade.

Figure 7 Comparison of BEMT simulation and the corresponding measurements for hover case (V = 0), (a) thrust (b) torque (see online version for colours)

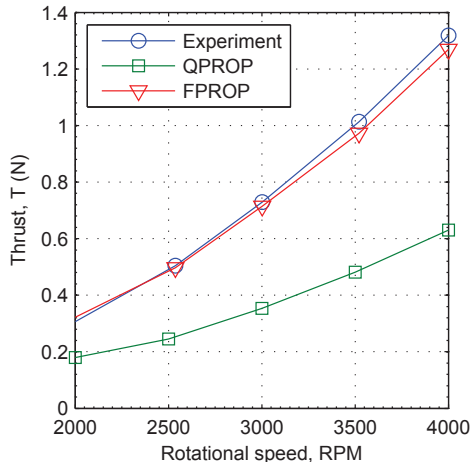

(a)

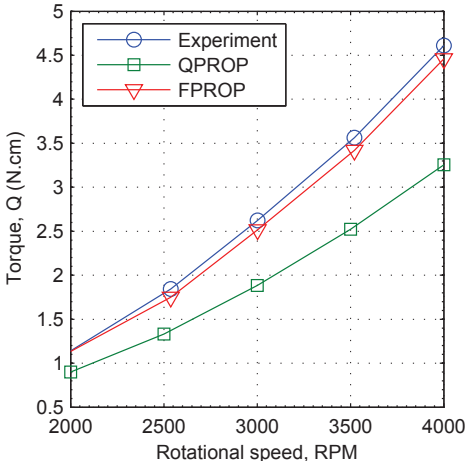

(b)

2.4 *Structural model (FBEAM)*

The structural analysis is based upon the use of anisotropic beam finite element model to determine the blade deflections during operation. The FBEAM consists of an integrated set of programs, which perform a two-dimensional cross-sectional analysis of the blade, followed by a one-dimensional finite element of a proprotor blade. A global coordinate system, shown in Figure 10 is used for the description of the blade geometry and the calculation of the loads. This is a right-handed Cartesian coordinates system where; the Y-axis is co-linear with the proprotor rotation axis and its positive in the direction of flight. The Z-axis is in the plane of rotation and points towards the blade tip. The X-axis is chordwise direction where the feathering axis is referred to. In this study, feathering axis was set at quarter-chord. BECAS (Blasques and Lazarov, 2012), a cross-sectional analysis tool which is developed at Denmark Technical University (DTU) was incorporated in this structural analysis program. The motivation of employing BECAS in this two-step structural model is due to the fact that BECAS has ability

to determine the cross section stiffness properties while accounting for all the geometrical and material induced couplings. These properties are also consequently utilised in the development of beam models to accurately predict the response of proprotor blades with complex geometries and made of advanced materials.

Figure 8 Comparison of BEMT simulation and the corresponding measurements with inflow (V = 16 m/s), (a) thrust (b) torque (see online version for colours)

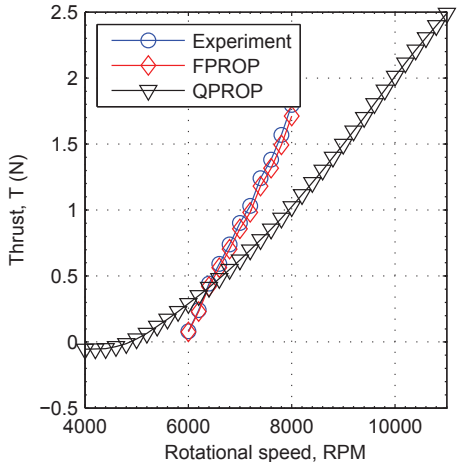

(a)

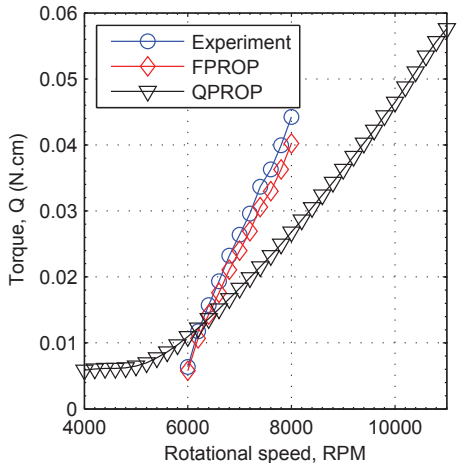

(b)

Figure 9 Global coordinate system of the blade

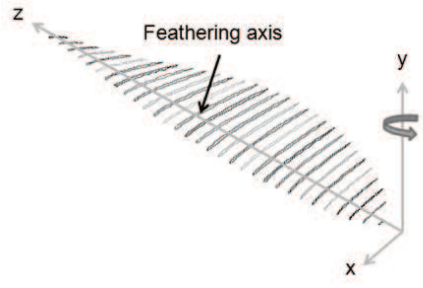

Figure 10 Finite element beam model and cross-sectional analysis

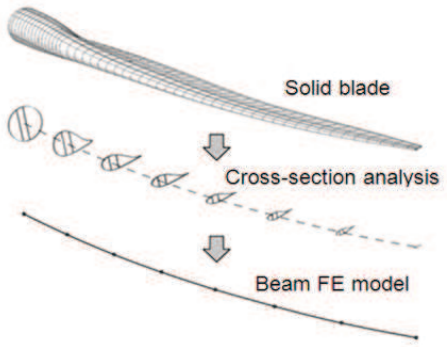

Figure 11 Cross section coordinate system, (a) forces and moments (b) strains and curvatures

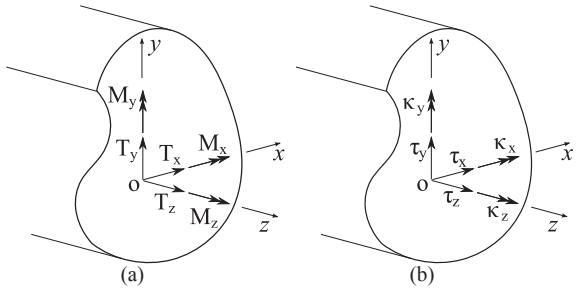

The linear relation between the cross section that generalised forces T and moments M [Figure 11(a)] and the resulting strains and curvatures [Figure 11(b)] is written in a stiffness form as follows:

$$\begin{pmatrix} T_x \\ T_y \\ T_z \\ M_x \\ M_y \\ M_z \end{pmatrix} = \begin{pmatrix} S_{11} & S_{12} & S_{13} & S_{14} & S_{15} & S_{16} \\ S_{21} & S_{22} & S_{23} & S_{24} & S_{25} & S_{26} \\ S_{31} & S_{32} & S_{33} & S_{34} & S_{35} & S_{36} \\ S_{41} & S_{42} & S_{43} & S_{44} & S_{45} & S_{46} \\ S_{51} & S_{52} & S_{53} & S_{54} & S_{55} & S_{56} \\ S_{61} & S_{62} & S_{63} & S_{64} & S_{65} & S_{66} \end{pmatrix} \begin{pmatrix} \tau_x \\ \tau_y \\ \tau_z \\ \kappa_x \\ \kappa_y \\ \kappa_z \end{pmatrix} \tag{12}$$

where S_{ij} is the sectional stiffness matrix. Using the sectional stiffness matrix and mass matrix obtained in BECAS, the elemental stiffness matrix and mass matrix are evaluated. Elastic energy and kinetic energy of the beam element are considered in order to compute the elemental properties. The final form of elastic energy and kinetic energy are written in equations (13) and (14), respectively.

$$K_e = \int_0^L B_T S B dz \tag{13}$$

$$M_e = \int_0^L N_T M_s N dz \tag{14}$$

where M_s sectional mass matrix, is the strain-displacement matrix and N is the polynomial matrix. The details equation used in these relationships, where no couplings included, are described in Kim et al. (2011). Global

stiffness of the blade is obtained through spanwise integration. As for the one-dimensional finite element, the rotating Timoshenko beam theory, detailed as in Subsection 2.4.1, is used for considering finite element analysis. Static equilibrium equations are solved with the geometric boundary conditions in order to compute the shape function. With the obtained shape function, the principle of virtual displacements is used to derive the elemental stiffness. And for the purpose of integration, a Gauss quadrature is used where for this study, four-nodes one-dimensional elements were chosen. For structural model validation, a static analysis on a rectangular planform with dimension (190.5 mm × 12.7 mm × 3.175 mm) was performed. Graphite-epoxy with material properties $E_{11} = 129GPa$, $E_{22} = 9.4GPa$, $E_{33} = 9.4GPa$, $G_{12} = 5.16GPa$, $G_{13} = 4.3GPa$, $G_{23} = 2.54GPa$, $\nu = 0.3$ and ρ = 1,550 kg/m^{3}was used. The ply angle with respect to pitch axis was 30°. The result obtained in FBEAM was validated by commercial structural analysis program namely MSc. Nastran and the validation result is illustrated in Figure 12.

2.4.1 *Rotating coupled Timoshenko beam*

As the blade is modelled as a rotating, cantilever Timoshenko beam, featuring flapwise bending – lagwise bending – torsion coupling, of arbitrary cross section and span, hence, expression of the elastic energy and kinetic energy of the beam element considering centrifugal force effect employed in the one-dimensional beam model is depicted in this section. By the consideration of coupling bend twist features, a wide range of structures can be then analysed, from beam-plates to monocoque box beams to fully build-in structures. However, the solid blade with rectangular planform made up of laminated composite material is a focus in this study. The expression for the potential energy due to flapwise bending, chordwise bending and torsion, U_{bt}, is given by:

$$\begin{aligned} U_{bt} = & \frac{1}{2}\int_0^L \int\int^A (\sigma_{zz}\varepsilon_{zz}) d\eta d\xi dz \\ = & \frac{1}{2}\int_0^L \int\int^A (E\varepsilon_{zz}^2) d\eta d\xi dz \end{aligned} \tag{15}$$

where A is the cross-sectional area and E is the Young's modulus.

The uniform strain, ε_0, and the associated axial displacement, u_0, due to the centrifugal force, $T(z)$, are related to each other as follows:

$$u_0^{'} = \varepsilon_0 = \frac{T(z)}{EA} \tag{16}$$

where the centrifugal force is expressed as follows:

$$T(z) = \int_z^L \rho A(R_0 + z)\Omega^2 dz \tag{17}$$

Here, ρ is the material density and R_0 is the hub radius.

Figure 12 FBEAM validation by MSc. NASTRAN, (a) flapwise deflection (b) torsion (see online version for colours)

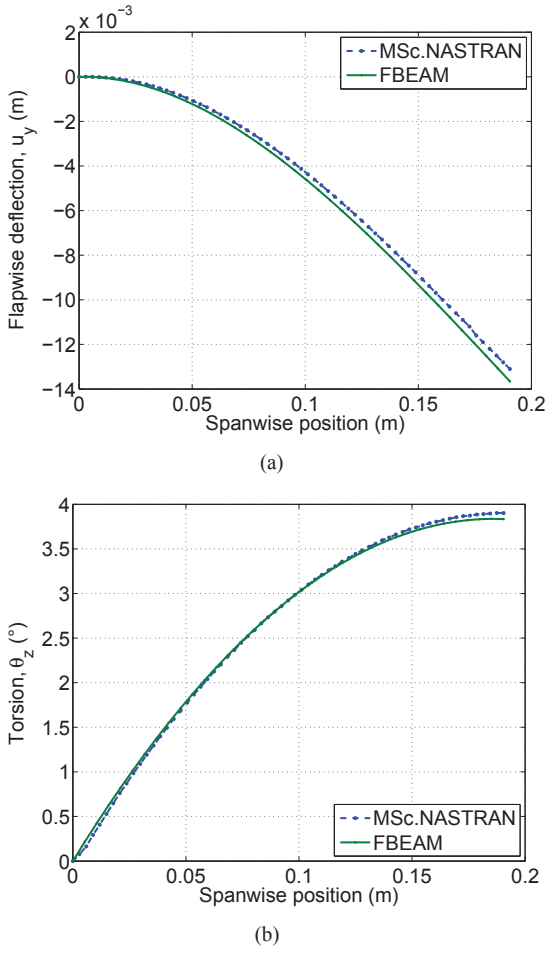

By substituting the component of the strain tensor with respect to spanwise into equation (15), taking integration over the blade cross-section, the following flapwise bending – lagwise bending – torsion potential energy expression is obtained:

$$\begin{aligned} U_{bt} = \frac{1}{2}\int_0^L \{ & T(z)[(v^{'})^2 + (w^{'})^2 + \frac{I_\alpha}{\rho A}(\psi^{'})^2 \\ & - 2e_1\varphi_y^{'} - 2e_2\varphi_z^{'}] + EI_{\xi\xi}(\varphi_y^{'})^2 \\ & + EI_{\eta\eta}(\varphi_z^{'})^2\} dz \end{aligned} \tag{18}$$

where I_α is the mass moment of inertia about the elastic axis, $I_{\xi\xi}$, $I_{\eta\eta}$ and $I_{\xi\eta}$ are the second moments of inertia, and J is the torsional rigidity constant. The expression for the potential energy due to shear, U_s, is given by:

$$\begin{aligned} U_s = & \frac{1}{2}\int_0^L \int\int^A (\tau_{z\eta}\gamma_{z\eta} + \tau_{z\xi}\gamma_{z\xi}) d\eta d\xi dz \\ = & \frac{1}{2}\int_0^L \int\int^A G(\gamma_{z\eta}^2 + \gamma_{z\xi}^2) d\eta d\xi dz \end{aligned} \tag{19}$$

where G is the shear modulus.

Substituting components of the strain tensor into equation (19), taking integration over the blade cross-section, the following expression for the potential energy due to shear is obtained:

$$U_s = \frac{1}{2}\int_0^L \{kAG(w' - \varphi_y')^2 + kAG(v' - \varphi_x')^2 + GJ(\psi')^2\}dz \tag{20}$$

where k is the shear correction factor, kAG is the shear rigidity, and GJ is the torsional rigidity of the beam cross-section. Summing equations (18) and (20) gives the total strain energy expression:

$$U = \frac{1}{2}\int_0^L \{T(z)[(v')^2 + (w')^2 + \frac{I_\alpha}{\rho A}(\psi')^2 - 2e_1\varphi_x' - 2e_2\varphi_y'] + EI_{\xi\xi}(\varphi_x')^2 + EI_{\eta\eta}(\varphi_y')^2 + kAG(w' - \varphi_y')^2 + kAG(v' - \varphi_x')^2 + GJ(\psi')^2\}dz \tag{21}$$

The load caused by the body forces generated by the central acceleration field, including centrifugal effects are included in the structural model. The stretching induced by the centrifugal inertia force due to the rotational motion causes the increment of the bending stiffness of the structure which naturally results in the variation of natural frequencies and mode shapes. Eigen-frequencies are calculated at different rotational speed. The Campbell diagram (Figure 13) is hence obtained to spot the dangerous crossings. Only the first six modal solutions are extracted. It can be seen that the eigen-frequencies of the modes display a small increasing trend with an increasing rotational speed, due to the stiffening effect which arises with the centrifugal loads. Several simulations were carried out to observe the operating condition and fibre orientation effect on blade deformations which later will be used for prediction in the design process. Figure 14 illustrates the effect of using anisotropic material on the bending and torsion deformations. Figure 15 demonstrates the deformations at different RPM. From the result in Figure 14 , it is found that the load in flapwise direction not only produces flapwise deflection but also torsion.

Figure 13 Variations of the lowest six natural frequencies of a rotating blade (see online version for colours)

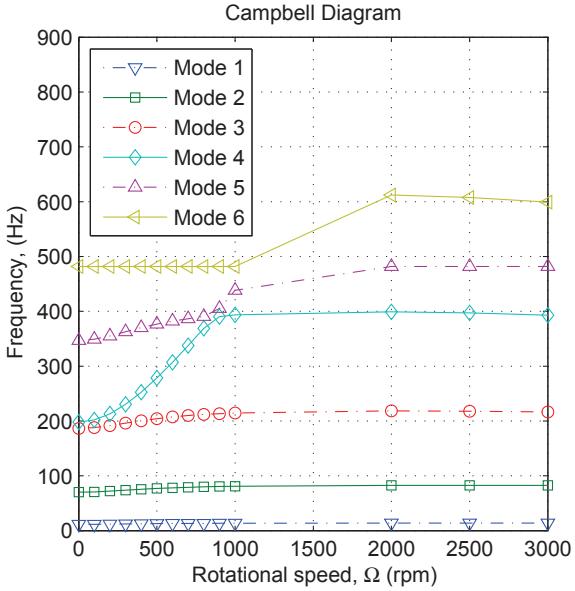

Figure 14 Effect of fibre orientation on blade deformations ($\beta = 15^0$, RPM = 1,000), (a) flapwise deflection (b) torsion (see online version for colours)

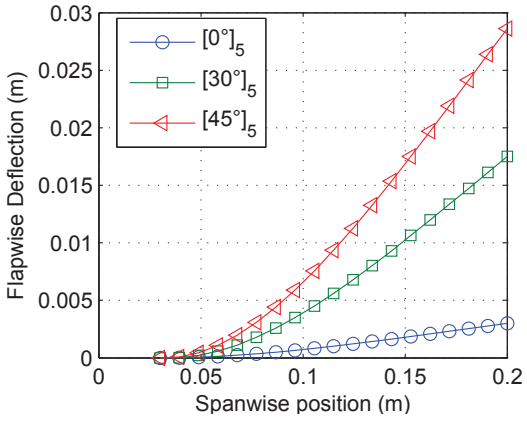

(a)

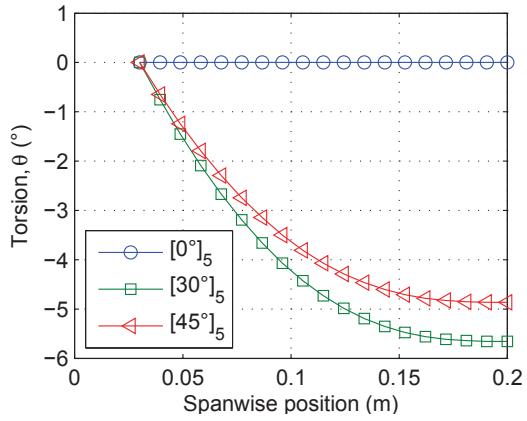

(b)

Figure 15 Blade deformations at different RPM (fibre angle = 30^0), (a) flapwise deflection (b) torsion (see online version for colours)

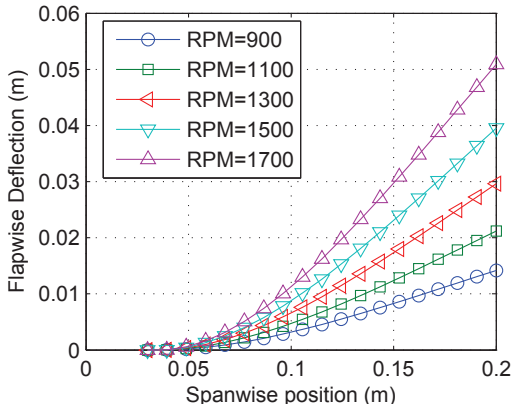

(a)

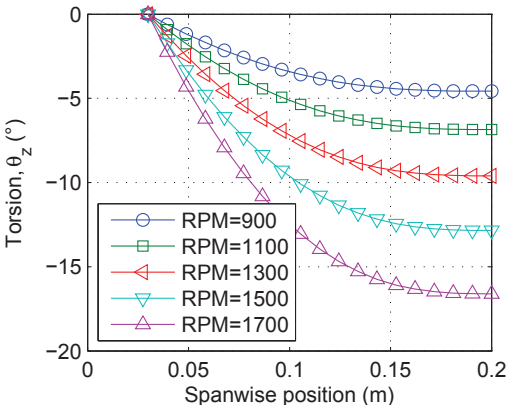

(b)

2.5 Coupled-aero-structure (FAE)

In order to compute the blade deformation under aerodynamic loadings, the coupled-aero-structure (CAS) model is developed. The coupled aero-structure of the proprotor combines the aerodynamic and structural analysis models. To begin with, the basic geometry (zero deflections) is assumed. Then the FBEAM structural model calculates the blade deformations under centrifugal loads. The deformed blade shape is used to update the aerodynamic model. The quasi-steady aerodynamic loads are computed for the update geometry, using the 2D aerodynamic theory based on stripwise manner model as described in Section 2.4. The aerodynamic loads are transferred to the beam FE nodes as concentrated forces. A new structural analysis is performed to calculate the deformed shape of the blade under the influence of aerodynamic and centrifugal loads. The variation of the blade twist angle along the blade is monitored for convergence. The aero-structural interaction is repeated until equilibrium between deformation and loadings is achieved. The convergence criteria set in this iterative process is 1×10^{-6}.

After convergence the proprotor performance characteristics are computed. The approach described above was applied to the constant chord untwisted 2-bladed system for UAV-sized proprotor made of laminate composite. The deflection results in two basic modes of deformation; spanwise bending and torsion. The effects of airfoil camber changes are not included in this study due to limitation in the modelling. Iteration 1 denotes the deflection due to centrifugal loads only and the rest include the aerodynamic loads. Figure 16 shows the corresponding variation of the calculated thrust and power coefficients.

The effect of single-step (SS) simulation, where the simulation stops at first iteration, and CAS simulation, where the iterative process is converged when equilibrium between deformation and loading is achieved, was investigated and the result is illustrated in Figure 17. A slight effect on deformation is observed which is approximately 1° in torsion and 5 mm in flapwise deflection at blade tip. However, the performance increases 3% by this effect.

Figure 16 Variation of thrust coefficient and power coefficient during the iteration, (a) thrust coefficient (b) power coefficient (see online version for colours)

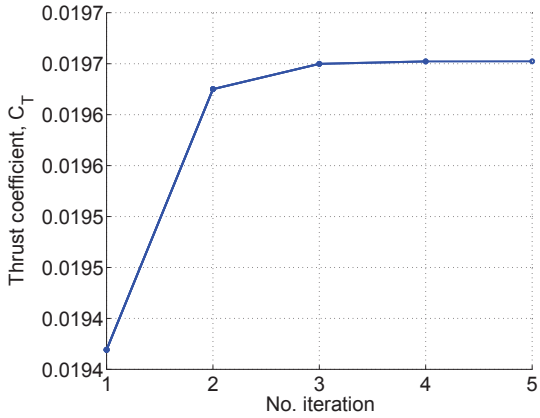

(a)

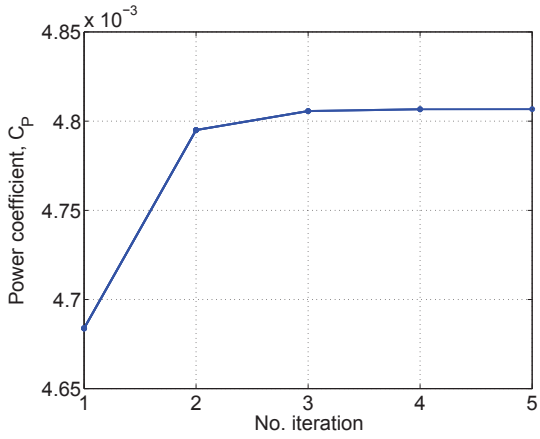

(b)

Figure 17 The effect of SS and CAS simulation on the blade deformations, (a) flapwise deflection (b) torsion (see online version for colours)

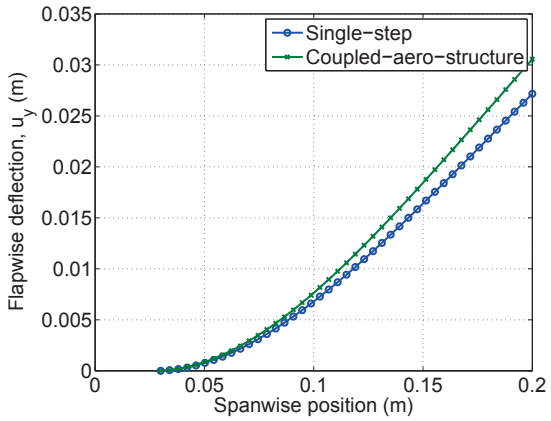

(a)

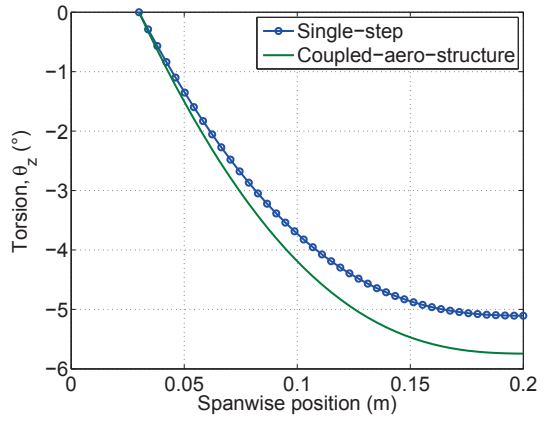

(b)

3 Experimental setup

Optical measurement techniques have been developing for a couple of years in applications of aerodynamics, materials and structure, such as holographic interferometry (HI), electronic speckle pattern interferometry (ESPI), projection moiré interferometry (PMI) and digital image correlation (DIC) (Williams, 1993). Fleming and Gorton (1998) obtained the 3-D deformation of rotor blade using PMI technique. However, it has low sensitivity for in-plane deformation and moderate for out-of-plane deformation. By contrast, DIC has a relatively high sensitivity that can reach 1/30,000 of the test field (Schmidt et al., 2003). Lawson and Jayant (2011) demonstrated the deformation of a rotating blade using DIC. The technique was found to have many advantages including high resolution results, non-intrusive measurement, and good accuracy over a range of scales. However, DIC needs a preprocessing which is to apply a stochastic speckle pattern to the surface by spraying it with a high-contrast and non-reflective paint. This complex painting will probably affect the stiffness of blade. Hence, in this study, laser distance sensor (LDS) was developed to measure blade deformation and validate the above numerical models. As is shown in Figure 18, the two LDSs are driven by track systems to scan the blade from blade root to tip with an incremental distance 2 mm.

Figure 18 LDS rig (see online version for colours)

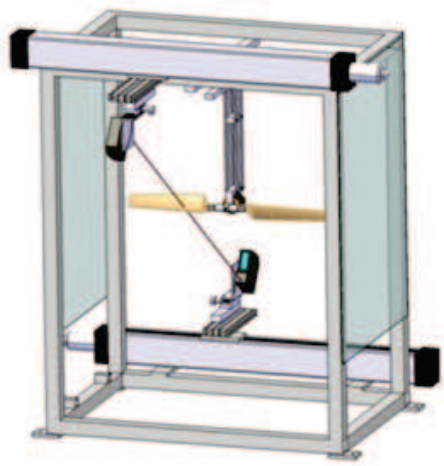

The LDS used in experiment is KEYENCE LK-G502. The distance of reference is 1,000 mm, and the range of measuring can be between –250 mm to 500 mm. The sampling frequency of this laser was selected as 10,000 Hz. At each blade section, the laser scans for two seconds. Finally, 20,000 data points were obtained totally for each section.

Figure 19 Post-processing procedure of LDS measuring

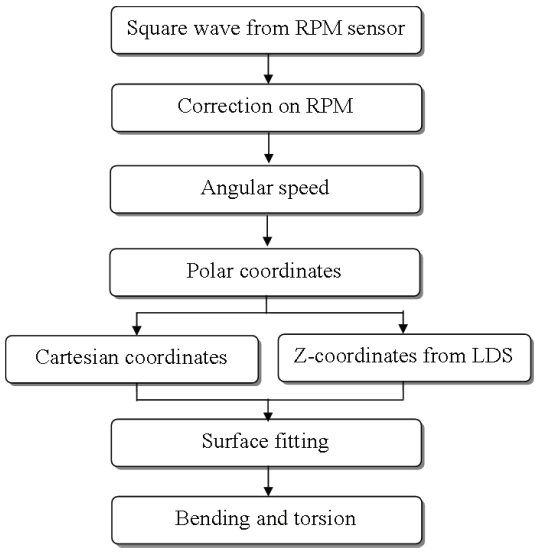

The post-processing of LDS measurement is shown in Figure 19. Firstly, LDS records the Z coordinates which is the distance from the position detected on blade surface to reference plane. Meanwhile, square wave in time domain is measured by RPM sensor. Then, average RPM and angular speed at each blade section can be extracted from the square wave. Furthermore, with the azimuth of feathering axis, polar coordinates is possible to be transferred to Cartesian coordinates X and Y. Combining coordinates X, Y and

Z, a polynomial surface fitting is performed to obtain the bending and torsion of rotating blade. Figure 20 shows the surface fitting visualisation of a deformed blade. To evaluate the flexible blade performance, the thrust and torque were measured using two transducers. The close-up of mounted blade is shown in Figure 21.

Figure 20 Surface fitting of a deformed blade (see online version for colours)

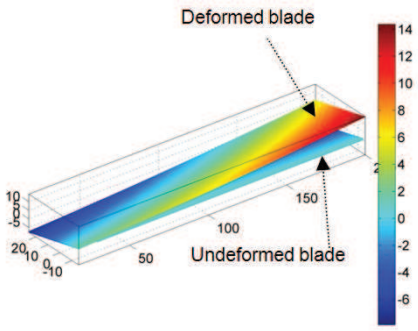

Figure 21 Close-up of mounted blade (see online version for colours)

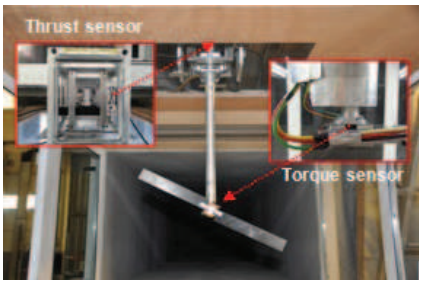

4 Result validations

The validation results in performance are shown in Figure 22. As can be seen, the FPROP agrees well with experimental data of thrust. However, it over-predicts the torque. Figures 23 and 24 show a good agreement of respectively flapwise deflection and torsion between the FAE simulation and the experimental data as obtained from LDS measurements. This is the result obtained for the blades clamped at collective pitch 35°. The fluctuations that can be observed through scattered plot of deformations are the results by the preliminary post-processing method. In this method, the deformation was extracted through the data interpolation at each section. Since the vibration of rotating blade probably generated uncertainty to the LDS data in spanwise, hence, the deformation exhibits unsmoothness in the plots. The maximum deviation of flapwise deflection and torsion between experimental measurement and FAE simulation are 8% and 6%, respectively, which are considerably acceptable.

Figure 22 Thrust and torque of rigid and flexible proprotor at different rotational speed (V = 0), (a) thrust (b) torque (see online version for colours)

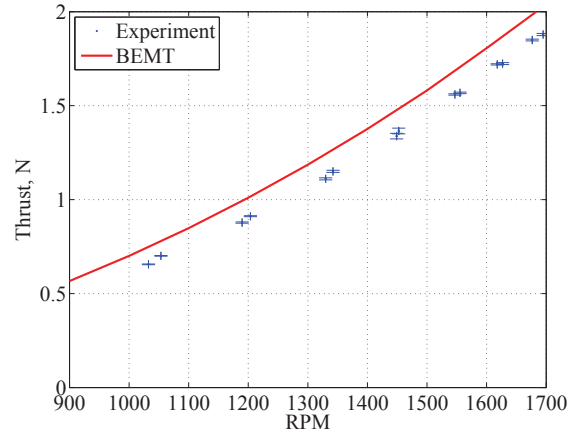

(a)

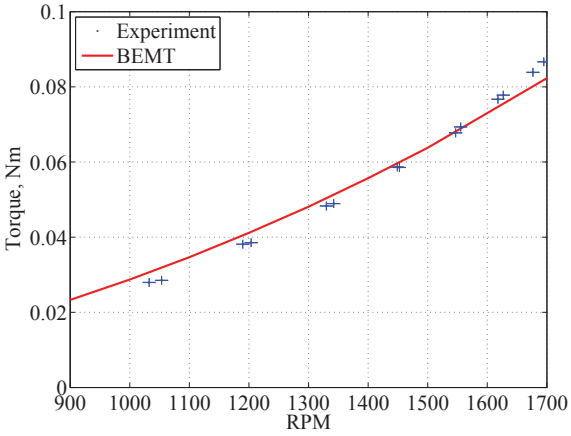

(b)

Figure 23 Comparison of flapwise deflection between FAE simulation and corresponding measurements (see online version for colours)

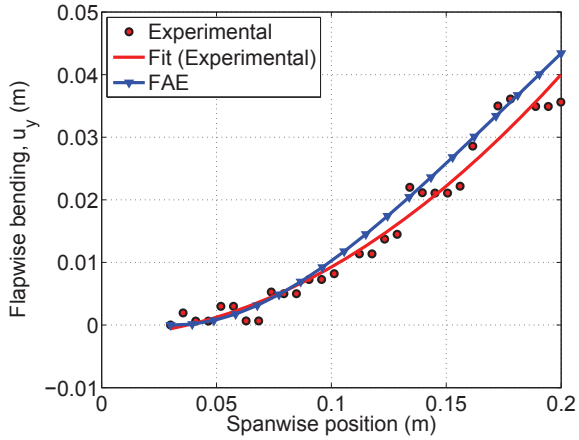

5 Conclusions

As conclusions, the evaluation of design techniques, both for the aerodynamic performance and for the structural behaviour of a composite flexible proprotor has been presented in rotor modes. The numerical model has capability of prediction in proprotor aerodynamics and structure. The model presents coupling between anisotropic beam finite element model and an aerodynamic model that takes into consideration the low Reynolds number aerodynamic. The influence of deformations is taken into account during the iteration procedure. The numerical model that utilises the above-described approach has also been experimentally validated by LDS technique and transducers of thrust and torque. Through validation results of both aerodynamic and structural model, it can be concluded that the developed numerical model is valid as a reliable tool for designing and analysing the proprotor made of composite material. Additionally, the developed structural model which uses cross-sectional analysis enables a more complex blade with highly-twisted and/or arbitrarily-shaped blades to be efficiently analysed. As perspectives, an investigation of static aeroelasticity on the UAV-sized flexible proprotor will be carried out using the validated numerical model. In future, the study will focus on propeller modes and optimisation in composite laminates to enhance the proprotor efficiency. Likewise, based on inverse method, the loads on blade are expectedly able to be deducted from blade deformation.

Figure 24 Comparison of torsion between FAE simulation and corresponding measurements (see online version for colours)

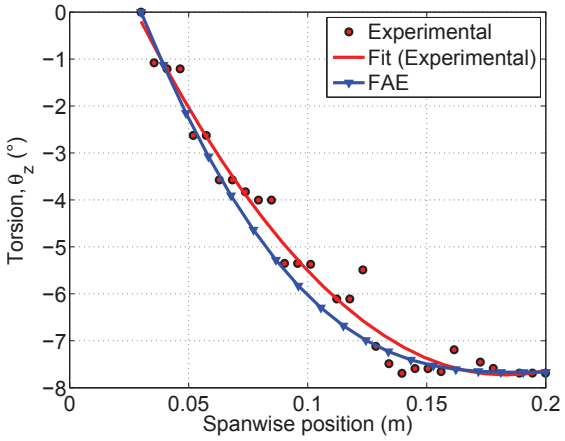

Acknowledgements

The authors would like to thank Rémy Chanton, Patrick Morel, Philippe Barricau, Serge Gerard, Patrick Cazenave, Philippe Mouligne, from Aerodynamic Laboratory of ISAE, and Xavier Foulquier from composite Laboratory of ISAE, for their technical advices and assistances. Likewise to China Scholarship Council (CSC) and Malaysian Ministry of Higher Education (MOHE) for their financial supports.

References

Adkins, C.N. and Liebeck, R.H. (1990) 'Design of optimum propellers', *Journal Propulsion and Power*, Vol. 10, No. 5, pp.676–682.

Blasques, J.P. and Lazarov, B. (2012) *Becas v2, a Cross-section Analysis Tool for Anisotropic and Inhomogeneous Beam Sections of Arbitrary Geometry*, Technical Report-R 1785, Technical University of Denmark.

Drela, M. (1989) *XFOIL: An Analysis and Design System for Low Reynolds Number Airfoil, Low Reynolds Number Aerodynamics*, USA.

Drela, M. (1990) *Elements of Airfoil Design Methodology in Applied Computational Aerodynamics*, Vol. 125, pp.167–189, AIAA Progress in Aeronautics and Astronautics Series.

Fleming, G.A. and Gorton, S. (1998) 'Measurement of rotorcraft blade deformation using projection moire interferometry', *Proceedings of the Third International Conference on Vibration Measurements by Laser Techniques: Advances and Applications, SPIE – The International Society for Optical Engineering*, Ancona, Italy, June.

Hein, B.R. and Chopra, I. (2007) 'Hover performance of a micro air vehicle: rotor at low reynolds number', *Journal American Helicopter Society*, Vol. 52, No. 9, pp.254–262.

Jones, R.T. (1990) *Wing Theory*, Princeton University Press, Oxford, UK.

Kim, T., Branner, K. and Hansen, A.M. (2011) 'Developing anisotropic beam element for design composite wind turbine blades', in *Proceedings of the 18th International Conference on Composite Material*, Jeju, Korea, August.

Laitone, E.V. (1997) 'Wind tunnel tests of wings at reynolds numbers below 70,000', *Journal Experiments in Fluids*, Vol. 23, No. 5, pp.405–409.

Lawson, M.S. and Jayant, S. (2011) Measurement of deformation of rotating blades using digital image correlation', *Structural Dynamics and Materials Conference, 52nd AIAA/ASME/ASCE/AHS/ASC Structures*, pp.1–15, Denver, Colorado, April.

Leishman, J. (2006) *Helicopter Aerodynamics*, 2nd ed., Cambridge, New York, USA.

McVeigh, M.A. and Rosenstein, H.J. (1983) 'Aerodynamic design of the XV-15 advanced composite tilt rotor blade', *39th Annual Forum of the American Helicopter Society*, pp.72–80.

Mohd-Zawawi, F., Morlier, J., Grondin, G. and Moschetta, J.M. (2012) 'Design of optimum torsionally flexible proprotors for tilt-body MAVs', *Journal Applied Mechanics and Materials*, Vol. 225, pp.281–286, DOI :10.4028/www.scientific.net/AMM.225.281, ISSN 1660-9336.

Nixon, M.W. (1998) *Improvements to Tilt Rotor Performance through Passive Blade Twist Control*, NASA Technical Memorandum 100583, pp.1–9.

Schmidt, T., Tyson, J. and Galanulis, K. (2003) 'Full-field dynamic displacement and strain measurement using advanced 3D image correlation photogrammetry: Part 1', *Journal Experimental Techniques*, Vol. 27, No. 3, pp.47–50.

Shkarayev, S., Moschetta, J.M. and Bataille, B. (2008) 'Aerodynamic design of micro air vehicles for vertical flight', *Journal of Aircraft*, Vol. 45, No. 5, pp.1715–1724.

Sunada, S., Sakaguchi, A. and Kawachi, K. (1997) 'Airfoil section characteristics at a low Reynolds numbers', *Trans. ASME: Journal of Fluids Engineering*, Vol. 45, No. 119, pp.129–135.

Taylor, J.R. (2006) *An Introduction to Error Analysis: The Study of Uncertainties in Physical Measurements*, University Science Books, Sausalito, California.

Thipyopas, C. and Moschetta, J.M. (2008) 'Experimental analysis of a fixed wing vtol. mav in ground effect', *International Journal of Micro Air Vehicle*, Vol. 2, No. 1, pp.33–53.

Williams, D.C. (1993) *Optical Methods in Engineering Metrology*, Chapman and Hall, London, UK.